

## **TECHNO-ECONOMIC FEASIBILITY ANALYSIS OF SOLAR INDUSTRIAL PROCESS HEAT USING PARTICLE THERMAL ENERGY STORAGE**

**Loiy Al-Ghussain**  
 Argonne National  
 Laboratory, Lemont,  
 IL 60439, USA

**Taylor Johnson**  
 University of Florida,  
 Gainesville, FL

**Janna Martinek**  
 National Renewable  
 Energy Laboratory  
 Golden, CO

**Zhiwen Ma**  
 National Renewable  
 Energy Laboratory  
 Golden, CO

### **ABSTRACT**

*U.S. industry sectors accounted for 33% of total energy consumption in 2021 according to the Energy Information Agency. Industrial process heat accounts for 70% of the industry energy use with application temperatures ranging from 60°–1100°C. Industrial processes heavily rely on fossil fuels including cheap coal or natural gas and differ widely in operating conditions and load requirements which makes them difficult to standardize and imposes challenges in decarbonization. To this end, we have developed a particle-based thermal energy storage (TES) technology integrated with renewable energy sources from concentrating solar thermal power (CST) and/or photovoltaic (PV) power. The particle TES system uses low-cost and highly stable silica sand and can provide industrial process heat (IPH) over a wide range of temperatures. The TES system can serve as a uniform energy supply configuration integrated with renewable power to supply 24/7 heat for industry decarbonization. This paper focuses on the Levelized Cost of Heat (LCOH) and investigated the sensitivity of the LCOH to various economic parameters including the capital costs of the particle-TES system and solar tower system. This paper shows the economic potentials of the particle-TES for IPH applications. Various scenarios of combined on-site CST, PV, electric heater, and TES system capacities were considered to determine configurations of the CSP/PV/TES system that could fulfill the heat demand with minor contributions from grid backup. Conditions necessary to approach an LCOH target of ~\$0.02/kWh were evaluated.*

**Keywords:** Thermal energy storage, industrial process heat, particle thermal energy storage, concentrated solar thermal

### **NOMENCLATURE**

$A_{hel}$	Total heliostat reflective area
$A_m$	Total area of PV panels
$A_{SB}$	Particle-steam boiler surface area
$C_{grid}$	Cost of grid electricity
$C_{tot}$	Total system capital cost
$CAP_{heater}$	Particle heater capacity
$CAP_{PV}$	PV capacity

$CAP_{TES}$	TES capacity
$DHI$	Diffuse horizontal irradiance
$DNI$	Direct Normal Irradiance
$D_{met}^t$	Demand met by solar/TES
$D_{ex,el}^t$	Excess electrical energy
$D_{ex,th}^t$	Excess thermal energy
$D_{def}^t$	Deficit thermal energy
$D_{th}^t$	Thermal demand
$E_{charge,grid}^t$	Thermal energy from grid electricity
$E_{charge,RES}^t$	Thermal energy from PV electricity
$E_{CSP,th}^t$	Thermal energy produced by CSP
$E_{PV,el}^t$	Hourly electrical PV energy
$E_{grid,el}^t$	Hourly electrical grid energy
$E_{th,grid}^t$	Hourly electricity drawn from the grid
$E_{St,th}^t$	Stored thermal energy in TES
$d$	Nominal discount rate
$f_{TES,loss}$	TES loss rate (fraction of stored thermal capacity per hour)
$GT_{PPA}$	Median grid electricity price
$GT^t$	Hourly grid tariff
$H$	Skip hoist tower height
$H_{tower}$	Solar tower height
$I_T$	Total solar radiation on the PV module
$I_{b,t}$	Total beam radiation
$I_{d,t}$	Total diffuse radiation
$LS$	Lifespan of the system
$m_{part}$	Skip hoist mass flow rate
$t$	Hour number
$t_{CSP,shutdown}$	CSP receiver shutdown period
$t_{CSP,start}$	CSP receiver startup period
$T_h$	Maximum hot particle temperature
$O\&M$	Operation and maintenance costs
$P$	Steam pressure within particle-steam boiler
$R_{PV,ex}$	Revenue from excess PV electricity
$T_{PV}$	Estimated PV cell temperature
$T_{Ref,STC}$	Reference cell temperature at standard test conditions
$TES_{size}$	TES thermal capacity
$\beta$	Fixed PV module tilt angle
$\beta_{ref}$	Temperature coefficient of the PV module
$\eta_{CSP}$	CSP efficiency

This material is declared a work of the U.S. Government and is not subject to Copyright protection in the United States.

$\eta_{heater}$	Electric particle heater efficiency
$\eta_{misc}$	Miscellaneous losses
$\eta_{PV, ref}$	Reference PV module efficiency
$\eta_{rec, therm}$	Receiver thermal efficiency
$\theta$	Time-dependent incidence angle

## 1. INTRODUCTION

Greenhouse gas emissions from industry account for a significant portion of the total emissions in the United States (around 24% in 2020) with direct emissions from the combustion of fossil fuels for heat and power being the main contributor. Industrial process heat applications consume almost 36% of the overall energy consumed by the manufacturing sector [1]. The potential for solar industrial process heat (SIPH) has become increasingly of interest as industries seek to reduce their reliance on fossil fuels, reduce their carbon footprint and adopt more sustainable practices.

The temperature requirements of an industrial process are important considerations when measuring heat demand and assessing solar applications for process heating. Some industrial applications including the steel industry require high temperatures, up to 1000°C [2]; however, operating temperatures for many industrial applications range from 60 to 250°C [3] and roughly 50% of the demand for process heat occurs at temperatures of 300°C or less [4] among the most energy-intensive U.S. manufacturing industries, including food and beverages and pulp and paper. Additionally, SIPH necessitates extensive study of process integration, opening the door for much-needed improvements in industrial heat systems' energy efficiency.

Electrification of industrial processes has also been proposed as a solution, but direct electrification using variable renewable energy resources such as solar and wind is challenging due to the need for a constant heat input to allow continuous operation. To overcome this, a combination of concentrated solar power (CSP), solar Photovoltaic (PV), and wind integrated with thermal energy storage (TES) has been proposed as a cost-competitive way to provide a steady, year-round supply of high-grade thermal energy [3]. Coupling renewables with TES makes it possible to generate thermal energy and electricity for industrial processes directly, while simultaneously storing energy for later use in the form of heat, enabling constant operation cycles. TES has significant advantages over other long-duration energy storage technologies, including cost-effectiveness, long operational lifespan, large energy storage capacity, and the ability to supply both thermal and electrical energy [5,6]. Several studies have explored the use of TES for SIPH applications [7–13]. Many of these studies utilized CSP for SIPH applications such as steam [14] or hot air [15] and used molten salts as a TES media.

The use of molten salts as a TES material presents several key challenges; molten salts freeze at low temperatures, become unstable at high temperatures, and are corrosive to metal containment materials [5,16–19]. In response to these challenges, significant efforts have been invested to assess and investigate other TES technologies such as phase change

material TES [10,20], and particle-based TES systems with either a fluidized bed heat exchanger [5,21–23] or a packed-bed heat exchanger [24]. For instance, González-Portillo et al. in [21,23] developed a model to investigate the techno-economic feasibility of particle-TES system with solar tower system and fluidized bed heat exchanger for electricity generation. They highlighted the potential of such a system with LCOE below 0.06 USD/kWh<sub>e</sub>. Whereas Trevisan et al. [24] investigated the use of packed bed TES with CSP system for electricity generation and developed a quasi-steady state model for the thermo-economics of the system. They concluded that the LCOE of 50 MW<sub>e</sub> CSP can reach down to 0.065 USD/kWh<sub>e</sub> with a capacity factor larger than 50%. Other studies utilized thermochemical storage, storing both the sensible heat and chemical energy in the particles [25,26]. Buck et al. [25] demonstrated the viability and potential of the use of thermochemical particle-based TES with a solar thermal system for electricity generation. Similarly Gorman et al. [26] presented the use of thermochemical particle-based TES with CSP integrated with a combined Brayton cycle. They concluded that their system could produce electricity with LCOE around 0.06 USD/kWh<sub>e</sub>.

The National Renewable Energy Laboratory (NREL) has developed a particle-based TES system based on silica sand with high thermal performance over a wide range of temperatures which makes it ideal for SIPH applications [5,16,17]. Ma et al. [5] presented the design and use of a solid particle thermal energy storage system with a solar tower system for power generation. Additionally, they investigate the effect of the thermal power generation cycle type on the electricity storage cost. They concluded that integrating the particle-TES with Brayton combined cycle achieves the lowest storage cost. Moreover, they highlighted the potential of the particle-TES system as a long-term energy storage system that could complete with battery storage systems. In another study, Ma et al. [27] presented the possibility of charging the solid particle TES using thermal energy from CSP or/and an electrical heater that can be powered using PV or cheap electricity from the power grid.

SIPH is an emerging technology with both economic and environmental benefits, particularly in applications like bauxite mining, steam generation, hot air supply, and cogeneration. Table 1 presents and overview of IPH industry use cases from literature review and industry surveys, and indicates potential methods for particle-based SIPH integration and discharge methods to serve these applications. To the best of our knowledge, the literature lacks studies that investigate the techno-economic feasibility of the use of PV/CSP systems with moving particle TES for industrial process heat. Hence, this study aims to: (1) Develop a tool to assess the potential of the particle-TES developed previously by NREL [5,27] for IPH applications; (2) Evaluate and assess the techno-economic feasibility of the particle-TES system via the Levelized Cost of Heat (LCOH) for a single example use case; and (3) Investigate the sensitivity of the LCOH to various economic parameters including the capital costs of the particle-TES system components.

**Table 1.** Scenarios using steam, hot air, or hot particles for industrial processes.

Heating Media	Applications	SIPH Discharge	Notes
Hot particles	Preheating ores for steel, alumina, cement production	Direct heating and discharge	Direct use of heated particles
Hot air	Material processing, drying, materials separation, etc.	Pressurized fluidized bed	Open cycle such as curing or drying
Steam	Broad applications in food processing, enhancing oil recovery, refining, etc.	Particle/steam boiler	Open or closed steam loop depending on the application
Cogeneration	Supply of steam, hot water, and power.	Particle/steam boiler	May have grid connection

## 2. TECHNO-ECONOMIC ANALYSIS OF SIPH FOR INDUSTRIAL STEAM SUPPLY

### 2.1 System Overview

The SIPH system with solid particle TES relies on thermal energy delivered directly by CSP systems or/and by an electric particle heater powered by electricity from PV systems or/and by the grid. The electric heater can be arranged in parallel or series with the solar receiver; however, only the parallel configuration is considered here. Generation 3 CSP technology has been applied for direct heating of particles in a solar tower system. Figure 1 shows a schematic diagram of the proposed SIPH system for supplying hot water or pressurized steam using a particle/water heater or particle/steam boiler. We analyze the potential of SIPH with solid particle TES for a specific use case of steam supply to an industrial facility in the southwestern U.S.

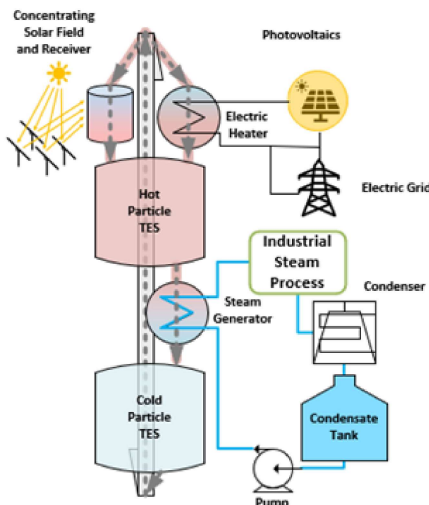


**Figure 1.** Schematic of the SIPH system investigated in this study for industrial hot steam supply.

An Excel-based optimal sizing and costing tool was developed to evaluate the techno-economics of these systems. The tool was used to optimally size six different system technology compositions discussed in Table 2, henceforth called “Scenarios”. Scenarios 3 and 4 fulfill the heat demand via the combined on-site CSP, PV, electric heater, and TES system, and draw electricity from the grid to heat particles only during those

hours in which the CSP/PV/TES system cannot meet the heat demand. Scenarios 1 and 2 allow the system to additionally charge thermal storage from grid electricity during any hours in which the electricity price falls below a designated cutoff. The model accounts for tradeoffs between capital cost for oversized CSP, PV, and/or TES components and the cost of grid electricity by minimizing the LCOH of the system as will be described below. Scenario 5 does not include CSP or PV assets and the system charges TES from the grid in any hour below a designated price threshold, uses the stored TES when available, and reverts to grid backup when TES is depleted.

**Table 2.** PV/CSP/TES scenarios evaluated in this study.

Scenario	CSP	PV	TES	TES Charging by Grid	Grid as Backup
Scenario#1	✓	✓	✓	✓	✓
Scenario#2	✓	✗	✓	✓	✓
Scenario#3	✓	✓	✓	✗	✓
Scenario#4	✓	✗	✓	✗	✓
Scenario#5	✗	✗	✓	✓	✓

Figure 2 shows the energy dispatch logic adopted here. The algorithm operates sequentially in each time step using the current TES state of charge, CST and PV availability, and price of grid electricity with no consideration of future resource availability or grid prices. The algorithm begins by assessing if the thermal energy generated by CST and PV is sufficient to meet the current thermal demand. If the total thermal energy exceeds the current demand, the algorithm first uses excess CST energy to charge the TES, subject to TES capacity limits. If excess CST energy is insufficient to fully charge the TES, the TES is also charged via the electric particle heater using excess PV and, in some cases, grid electricity (if grid charging is enabled in the scenario, the current electricity price is below a user-defined cutoff, and the excess PV electricity is less than the heater capacity). If the total thermal energy generated by the CST and PV/heater is insufficient to meet the current demand, the algorithm checks if the current grid price exceeds the user-defined cutoff price for grid charging. If so, the remainder of the thermal demand is covered by TES and supplemented with grid electricity only if the stored thermal energy is insufficient to meet the demand. If the grid price is below the charging cutoff and grid charging is enabled in the scenario, the particle heater

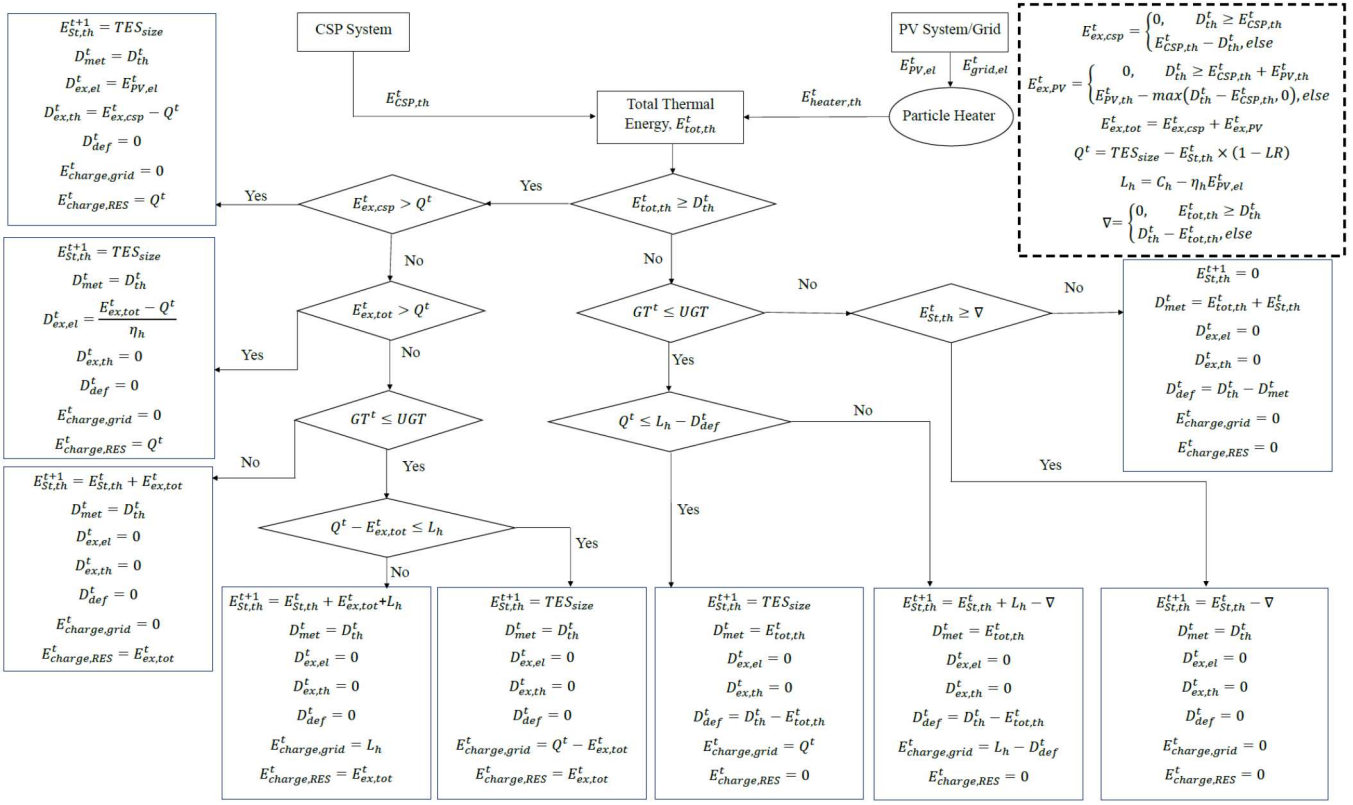


**Figure 2.** Energy dispatch strategy for SIPH system with solid particle TES

operates at full capacity, drawing energy from both PV and grid sources to satisfy the remaining thermal demand and charge the TES if possible. All scenarios presume the price of grid electricity is fixed at any given hour and that there is no feedback between electricity utilization and electricity price.

## 2.2 Annual Performance Analysis

For any given heat demand profile and set of component sizing parameters (e.g., CSP field and receiver capacity, PV capacity, TES capacity), a simplified hourly time-series annual performance analysis was conducted to estimate the hourly production from the CSP and PV technologies, TES charging/discharging, and cost of grid electricity requirements. The electrical energy produced by PV system ( $E_{PV,el}$ ) was estimated using:

$$E_{PV,el} = \eta_{PV,Ref} \left( 1 - \beta_{Ref}(T_{PV} - T_{Ref,STC}) \right) I_T A_m \eta_{misc} \quad (1)$$

where  $\eta_{PV,Ref}$  is the reference PV module efficiency,  $\beta_{Ref}$  is the temperature coefficient of the PV module,  $T_{PV}$  is the estimated PV cell temperature,  $T_{Ref,STC}$  is the reference cell temperature at standard test conditions,  $A_m$  is the total area of the PV panels, and  $\eta_{misc}$  accounts for miscellaneous losses including inverter and shading losses. The total solar radiation incident on the PV module ( $I_T$ ) is the sum of normal and diffuse components and estimated using the equations below where  $DNI$  is the direct

normal irradiance,  $DHI$  is the diffuse horizontal irradiance,  $\beta$  is the fixed PV module tilt angle, and  $\theta$  is the time-dependent incidence angle.

$$I_{b,t} = DNI \cos(\theta) \quad (2)$$

$$I_{d,t} = DHI \frac{1 + \cos(\beta)}{2} \quad (3)$$

The electrical energy produced by the PV system was converted to thermal energy assuming a fixed heater efficiency ( $\eta_{heater}$ ).

The CSP output is estimated based on the DNI, total heliostat reflective area ( $A_{hel}$ ), time-dependent solar field optical efficiency ( $\eta_{CSP}$ ), and an assumed fixed receiver thermal efficiency ( $\eta_{rec,therm}$ ).

$$E_{CSP,th} = DNI A_{hel} \eta_{CSP} \eta_{rec,therm} \quad (4)$$

The solar field layout and efficiency were determined via NREL's SolarPILOT software. The field performance was simulated at a set of zenith and azimuth angles over the course of the year, and then the field efficiency was interpolated to an hourly time series. As it was infeasible to fully couple the field layout and efficiency calculations to iterations over CSP capacity in the Excel-based tool, a field layout was initially simulated for a single CSP field/receiver thermal capacity for each scenario, and then selection of component capacities was carried out assuming the same field efficiency would apply to all CSP

thermal capacities considered during optimization in that scenario. The initial field efficiency was based on a heliostat field nominally sized to provide three times the thermal peak demand at design point conditions and the tower height was optimized within SolarPILOT for the given capacity. After the optimization algorithm determined the optimal CSP field size, the thermal efficiency used in the Excel model was updated based on the new size for the final analysis. This simplification does not fully account for the change in field efficiency that results from a change in CSP thermal capacity during optimization but is a reasonable first approximation when applied over a limited range. The CSP receiver thermal output calculated from the equation above was reduced in the first time period of operation after a period of zero DNI (for receiver startup) and in the last time period of operation before a period of zero DNI (for receiver shutdown) using fixed ramp rates ( $t_{CSP,start}$ ,  $t_{CSP,shutdown}$ ).

Base case operational assumptions are provided in Table 3. All CSP field design and performance parameters not specified here were set to SolarPILOT default values, and the grid charging price cutoff shown in Table 3 is relevant only in Scenarios 1, 2, and 5.

**Table 3.** Base case performance parameters [27–33].

PV and electric heater		CSP and TES	
Parameter	Value	Parameter	Value
$\eta_{PV,Ref}$	0.216	Heliostat size	6m x 6m
Tilt angle ( $\beta$ )	47°	Configuration	North Side
$\beta_{Ref}$	0.0034 1/K	$\eta_{rec,therm}$	90%
$T_{Ref,STC}$	25°C	$t_{CSP,start}$	12 min
$\eta_{misc}$	0.85	$t_{CSP,shutdown}$	12 min
$\eta_{heater}$	0.99	$f_{TES,loss}$	0.025 % / hr
Grid charging cutoff price	0.02 \$/kWh		

As described above, the available PV/heater and CSP thermal output in any hour was first used to satisfy the heat demand in that hour, and excess heat generation was used to charge thermal storage (subject to the thermal storage capacity limit). Stored thermal energy was subject to a thermal loss defined by a fixed fraction of the stored thermal capacity per hour ( $f_{TES,loss}$ ), and thermal energy was dispatched during any time period in which insufficient PV/heater and CSP thermal output was available to meet the heat demand. Excess CSP thermal output that would exceed the TES capacity was curtailed and provided no value to the system. Excess PV electrical output that could not be used to charge TES was sold back to the grid at an assumed purchase price. Note that this presumes that excess PV would have value to the grid at the time when it is generated, which may not be the case in future grid scenarios. In Scenarios 1, 2, and 5, the thermal storage was also charged from the grid during any hour with unused TES capacity in which the electricity price was below a given price threshold. Note that the operational strategy in these grid-charging scenarios does not give any consideration to future PV and CSP availability, and

thus the model cannot choose to forego current grid charging in favor of anticipated future PV or CSP thermal output that is expected to fill the TES capacity later in the day. This operational simplification will likely result in under-utilization of the on-site solar resources in Scenarios 1 and 2, and future work could enhance these simple operational strategies via forward-looking dispatch optimization approaches.

### 2.3 Economic Analysis and Component Sizing

The tool seeks to minimize the levelized cost of heat (LCOH) of the system via selection of the CSP, PV, and TES capacities for each scenario. LCOH was defined as:

$$LCOH = \frac{C_{tot} + C_{O\&M} + C_{grid} - R_{PV,ex}}{\sum_{y=1}^{LS} \frac{\sum_{t=1}^{8760} D_{th}^t}{(1+d)^y}} \quad (5)$$

$$C_{O\&M} = \sum_{y=1}^{LS} \frac{O\&M}{(1+d)^y} \quad (6)$$

$$C_{grid} = \sum_{y=1}^{LS} \frac{\sum_{h=1}^{8760} GT^t \times E_{th,grid}^t / \eta_{heater}}{(1+d)^y} \quad (7)$$

$$R_{PVexcess} = \sum_{y=1}^{LS} \frac{\sum_{h=1}^{8760} GT_{PPA} \times D_{ex,el}^t}{(1+d)^y} \quad (8)$$

Here the LCOH was defined to include the total installed capital cost of all components ( $C_{tot}$ ), annual O&M costs ( $C_{OM}$ ), annual costs of charging TES from grid electricity ( $C_{grid}$ ), and is reduced by revenue derived from sales of excess PV electricity ( $R_{PVexcess}$ ) at an assumed average price. The hourly price of grid electricity was set via Eq. (9):

$$GT^t = (LMP^t / \text{median}(LMP^t)) \times GT_{PPA} \quad (9)$$

where  $LMP^t$  is the time-dependent locational marginal electricity price for the selected location. This profile was normalized around a defined median grid price ( $GT_{PPA}$ ) to enable sensitivity analysis around average grid price assumptions, and the base case average grid price was set to 0.04 \$/kWhe. The time-dependent grid electricity requirements were calculated from the annual analysis described in Section 2.2, the base-case plant lifetime ( $LS$ ) was set to 25 years [30], and the discount rate ( $d$ ) was assumed to be 10%.

Table 4 provides the base case capital cost and O&M cost assumptions for all system components. Base case specific costs of the solar components (CST heliostat field, CST receiver, PV field) are similar to the DOE SunShot 2030 “high-performance” case [30]. These costs and the assumed receiver efficiency in Table 3 represent future target values. Designs for system components including the particle heater and TES were described in prior work [32, 33] and cost functions for the particle heater, TES, skip hoist, and discharging components were derived by iterating detailed component design calculations

**Table 4.** Empirical formulas and base case cost inputs used to estimate the capital cost and O&M cost of SIPH components.

System	Subsystem	Empirical formulas or cost assumptions
CSP Field	Heliostat	$C_{hel} = 80 \times A_{hel}$ , including site preparation, land cost and heliostat cost [30]
Particle Receiver	Receiver	$C_{rec} = 124 \times CAP_{CSP}$ [16]
	Tower	$C_{tower} = 1194000 \times e^{(0.0124 \times H_{tower})}$ [23]
PV	-	$C_{PV} = 773.7 \text{ \$/kW} \times CAP_{PV}$ , [30]
Particle Heater [32]	Heating wire	$C_{wire} = 21192 CAP_{heater}$
	Insulation material	$C_{Insulation} = 291.71 CAP_{heater}$
	Refractory material	$C_{Refractory} = 344.67 CAP_{heater}$
	Control box	$C_{control} = 0.2 \times (C_{Refractory} + C_{Insulation} + C_{wire})$
TES [32]	Silo containment	$C_{const} = 217930.89 CAP_{silo}^{0.26}$
	Insulation material	$C_{Insulation} = a \times T_h - b$ $a = -4.86 \times 10^{-6} \times CAP_{silo}^2 + 0.54897 \times CAP_{silo} + 323.42$ $b = -0.001 \times CAP_{silo}^2 + 153.065 \times CAP_{silo} + 97539.568$
	Media	$C_{media} = 35 CAP_{silo}$
Skip Hoist [32]	-	$C_{skip} = a \times \dot{m}_{part}^2 - b \times \dot{m}_{part} + c$ $a = 10.352 \times \ln(H) - 36.649$ , $b = 8.3029 \times H - 462.64$ $c = 1787.962 \times H + 294134.6$
Particle-Steam Boiler	U-tube HX	$C_{SB} = (4.22P^2 + 30.8P + 1157) \times A_{SB} + 250.92P^2 + 1831.9P + 68784$
O&M	-	CSP: 9 \\$/kW <sub>th</sub> [32], PV: 5 \\$/kW <sub>dc</sub> [32], All other components: 5% of capital cost (per year)

described in [32] over a range of unit capacity, pressure, and temperature conditions. The functions shown in Table 4 were fit to the resulting set of calculated costs. Note that the total capital cost used in the LCOH calculations here accounts for only the bare-erected component costs, and did not include estimates for site, building, system integration, contingency, EPC cost, debt costs, sales tax, etc.

## 2.4 Case Study Assumptions

Sizing of the CSP field, PV array, and TES capacity were selected by minimizing the calculated LCOH for each scenario. All Scenarios have the same objective and constraints but differ on the available set of sizing variables as shown in Table 5. The selected values of the sizing variables change depending on the system technologies and configuration for each scenario. The sizing that minimizes the calculated LCOH was found using the GRG nonlinear solver tool in Excel.

**Table 5.** Sizing variables for each scenario

Scenario	System configuration	Variables
#1	PV+CST+TES+ Grid	$A_{hel}, CAP_{PV}, CAP_{TES}$
#2	CST+TES+Grid	$A_{hel}, CAP_{TES}$
#3	PV+CST+TES	$A_{hel}, CAP_{PV}, CAP_{TES}$
#4	CST+TES	$A_{hel}, CAP_{TES}$
#5	Grid+TES	$CAP_{TES}$

In the case study considered here, the SIPH system is designed to supply a steam demand with the assumptions

presented in Table 6. The required thermal load ( $D_{th}$ ) is calculated to be approximately 18 MW<sub>th</sub> based on the required steam flow rate and temperature conditions. The hot particle TES temperature was assumed to be 750°C for TES sizing, TES insulation, and heat exchanger sizing and cost calculations. This high temperature was selected to limit the TES footprint and cost, despite the low-temperature IPH demand.

**Table 6.** Case study assumptions

Parameter	Value
Steam flow rate	6.3 kg/s
Water inlet pressure	1 atm
Steam outlet pressure	1.034 MPa
Water inlet temperature	25 °C
Steam temperature	260 °C
Plant operation	24/7

The location analyzed in this study is in southeast California just south of Death Valley National Park and receives annually 2,822 kWh/m<sup>2</sup> and 2,107 kWh/m<sup>2</sup> of direct normal and global horizontal solar irradiance, respectively. All time-series annual performance calculations were based on 2021 solar resource data for the selected location obtained from the National Solar Radiation Database (NSRDB) [34]. The locational marginal electricity price was set from the historical 2021 hourly marginal electricity price obtained from CAISO [35] for a node in Southern CA near this location. Figure 3 illustrates the base case grid electricity price signal used in the case study. The price

signal was scaled to a median price of 0.04 \$/kWh based on Eq (9). Note that the scale in Figure 3 is saturated at 0.15 \$/kWh for visibility and high price outliers exist in the data. While this analysis serves as an example for a single use-case and location, the time variation of electricity price can be expected to change as the composition of the grid shifts toward a greater fraction of renewable technologies in the future. All results shown here are sensitive to assumptions regarding hourly cost of grid electricity.

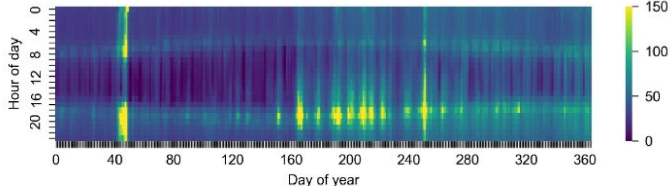


**Figure 3.** Base case grid electricity price signal (\$/MWh<sub>e</sub>).

### 3. RESULTS AND DISCUSSION

Sizing the SIPH system is crucial to ensure technoeconomic competitiveness by minimizing the LCOH while limiting the curtailment of CSP and PV generation. The capacities of each system which minimize the calculated LCOH for Scenarios 2, 4, and 5 are shown in Table 7. Note that Table 7 does not include the results from Scenarios #1 and #3. In these scenarios the system was allowed to include a PV array; however, the solver reduced the PV capacity to zero to minimize LCOH and thereby replicated the results of Scenarios #2 and #4, respectively. As mentioned in Section 2, the base case capital costs used here do not account for contingency, EPC cost, or sales tax and thus may underestimate the true LCOH. If a 7% contingency cost, 13% EPC cost, and 5% sales tax on 80% of the total direct cost are included in the capital cost (based on default values from NREL's System Advisor Model (SAM) v 2022.11.21 CSP molten salt power tower case), the LCOH for Scenarios #2 and #4 in Table 7 would increase by roughly 12%.

**Table 7.** Optimal configurations of SIPH for industrial steam supply case study.

Variable	Scenario #2	Scenario #4	Scenario #5
$A_{hel}$ (m <sup>2</sup> )	94060	100385	-
Max CSP output (MW <sub>th</sub> )	63.0	66.9	-
$CAP_{PV}$ (MW <sub>e</sub> )	-	-	-
TES Duration (hours)	32.5	26.6	6.0
TES Capacity (MWh <sub>th</sub> )	585	479	108
Annual grid fraction	0.14	0.07	-
LCOH (\$/kWh <sub>th</sub> )	0.0264	0.0264	0.0482

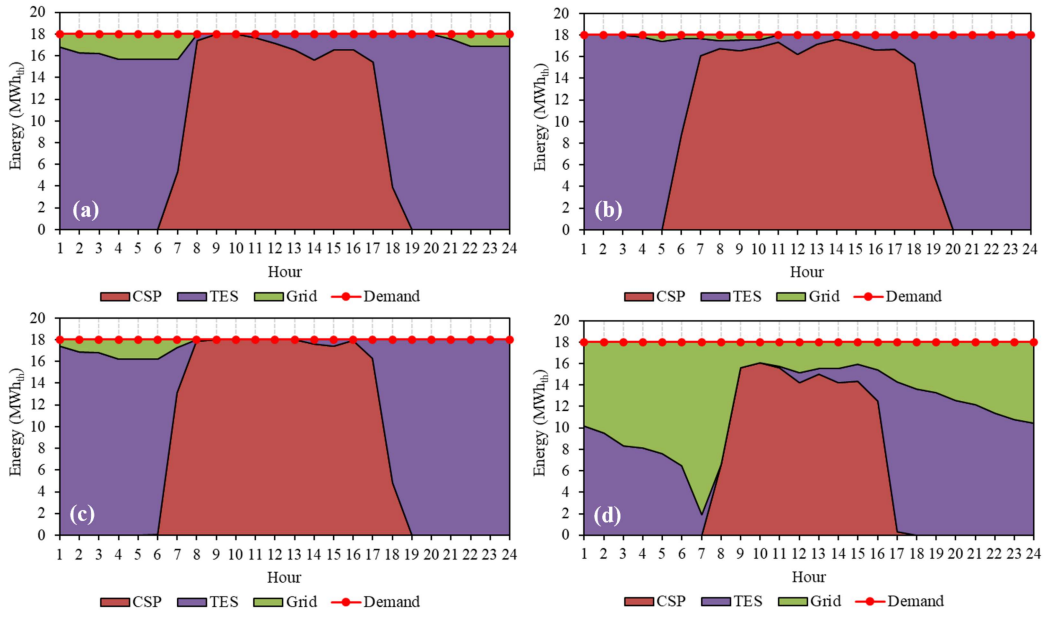
For the base case input parameters and electricity price signal, Scenarios #2 and #4 produced the lowest calculated LCOH to supply steam. In Scenario #4 the grid is used only for running the electric heater during the deficiency periods when TES is depleted, while Scenario #2 charges TES from the grid anytime the price of grid electricity falls below 0.02 \$/kWh<sub>th</sub>. Note that the CSP capacity is provided in terms of both the

heliostat field area (the design parameter used in the optimization) and the corresponding maximum thermal output from the annual calculations. The CSP capacity in Table 7 corresponds to a solar multiple of approximately 3.5 and 3.7 for Scenarios #2 and #4, respectively, relative to the 18 MW<sub>th</sub> heat demand. Scenario #4 provides 93% of the heat demand from the on-site CST-TES resources and only relies on grid backup for the remaining 7%. The similar CSP and TES sizing selected in Scenarios #2 and #4 suggest that a large heliostat field and receiver size are required to minimize use of the most expensive grid electricity, and that the ability to charge from low-cost grid electricity (which, for the price signal use here, typically occurs during mid-day hours with strong solar resource) does not provide substantial cost benefits. However, the simplified operational strategies used in Scenario #2 force the system to charge from the grid below the 0.02 \$/kWh<sub>th</sub> price threshold and can result in preferential use of grid electricity and additional CSP curtailment, and thereby increase the fraction of the total heat supplied by the grid. The balance between large on-site resources and grid backup can be expected to be sensitive to assumptions surrounding both grid electricity price and component costs.

Scenario #5 excludes both CSP and PV resources and is only allowed to charge storage below the designated hard price cutoff of 0.02 \$/kWh<sub>th</sub> in these calculations. This likely overestimates the minimum possible LCOH for a grid-tied TES system. Realistically, there may be times when it would be optimal to charge storage at higher grid prices, for example, during the summer months where there is a very high maximum price but the minimum price rarely falls below the cutoff used here. The simplistic strict operation constraints of Scenario #5 here do not provide the system flexibility to adapt to these variations in price.

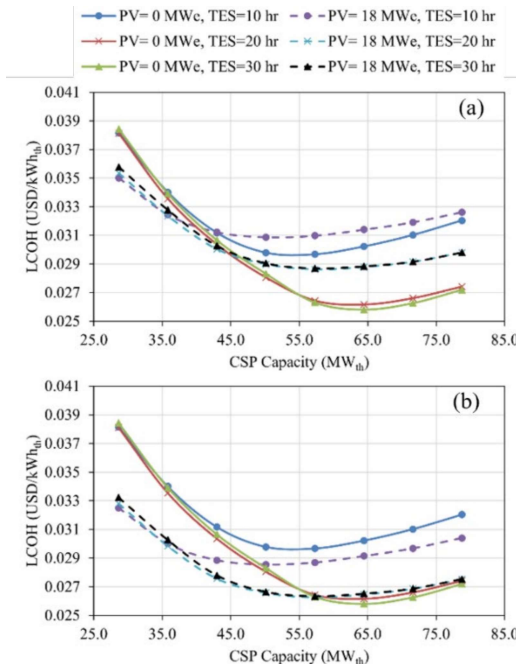
Figure 4 illustrates the average hourly demand profile and quantities met by CST, TES, and the grid for Scenario #4 averaged over all days within each of four months. CST is the dominant energy source during midday hours throughout the spring, summer, and early fall and directly provides the majority of the mid-day heat demand while the TES acts as a load-shifting mechanism to satisfy the demand outside the production hours for the CST field by storing excess heat during peak hours. During winter months (Figure 4 (d)) there is not enough stored thermal energy to meet the demand, forcing the system to purchase electricity from the grid to satisfy the deficit. Nearly 35% of the system's energy was derived from the grid for the month of December, compared to an annualized average of 7%. The relative sizing of CST and PV components was optimized relative to the specific selected grid price signal; thus, a grid price signal with a higher electricity price in the winter months would likely have resulted in larger CST and PV installations to avoid this extensive usage of the grid electricity.

Optimal component sizing evaluated under the base-case component cost assumptions in Table 7 excluded PV from the solution; however, this conclusion is, in part, a result of aggressive CSP cost assumptions relative to current costs and may not hold true under a broad range of cost assumptions.



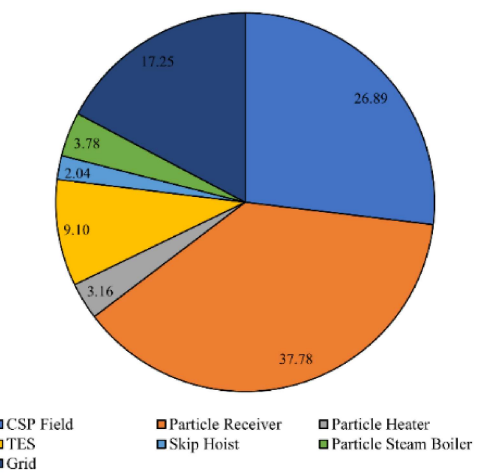
**Figure 4.** Average hourly profile of demand, amount of energy met by CSP directly, amount of energy met by TES and amount of energy met by grid directly in each season; a) March, b) June, c) September, and d) December.

Figure 5 illustrates sensitivity of LCOH to PV, CST, and TES capacity (assuming fixed CSP field efficiency) at the base-case cost assumptions (Table 4) and at reduced PV costs. At reduced PV capital cost relative to CST (Figure 5b), the LCOH of the hybrid PV-CST-TES system is, for many conditions, lower than the LCOH of the analogous CST-TES system and thus optimization of the component capacities under these assumptions may lead to the inclusion of a PV array.



**Figure 5.** Sensitivity of LCOH to CSP, TES, and PV sizing for (a) base-case and (b) reduced PV capital cost (570 \$/kW<sub>e</sub>)

The cost breakdown of the SIPH system for Scenario #4 in Figure 6 shows that more than 64% of the total cost is associated with the solar receiver and heliostat field costs. Grid electricity costs over the 25-year lifetime of the plant represent 17% of the total capital costs. TES accounts for only 9% of the capital expenditure despite a large TES capacity (26.6 hours), owing to the low cost of particle TES relative to traditional molten salt or other storage technologies. The relatively low cost of particle TES facilitates the economic viability of the large TES capacity necessary to support a high-capacity factor.



**Figure 6.** Cost breakdown of optimal CST+TES (Scenario #4) SIPH subsystems

Figure 7 shows the possible change in LCOH of a SIPH system for industrial steam supply based on cost reductions in

various components and indicates that the LCOH is most sensitive to assumptions regarding heliostat cost followed by thermal efficiency of the solar receiver and the grid pricing. The system design (i.e. the sizing of the CST field, PV array, and TES capacity) was held constant during this sensitivity analysis, and thus the results shown here do not account for potential changes in optimal design that would result from higher/lower cost parameters. Thus, a higher grid electricity price here simply increases the total cost of electricity purchases, whereas a system optimized around this higher grid price would likely result in larger on-site CST, PV, and TES installations and thereby lower reliance on grid electricity. Conversely, a system optimized around a higher heliostat or receiver cost would likely lead to a smaller CST installation and thereby larger reliance on grid electricity.

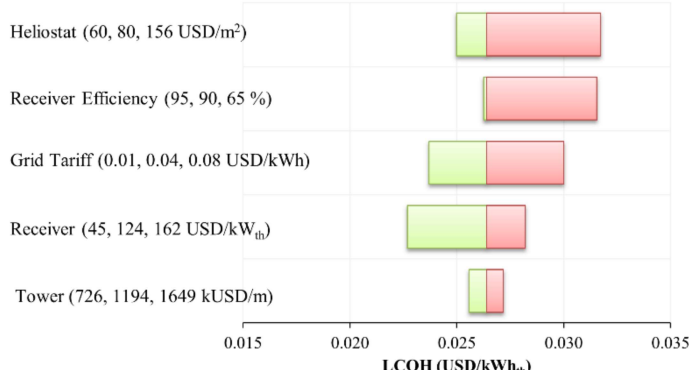


**Figure 7.** Sensitivity of the LCOH of the optimal CST-TES (Scenario #4) SIPH system

#### 4. CONCLUSION

This work developed a tool to assess the techno-economic potential of particle-TES systems for IPH applications and demonstrated the calculations for an example use case of supplying hot steam for industrial applications. Various scenarios of combined on-site CST, PV, electric heater, TES, and grid-connected systems were considered to fulfill the heat demand. The results focus on the Levelized Cost of Heat (LCOH) and include a simplified annual performance analysis and TES dispatch strategy to connect the sizing of the CST, PV, electric heater, and TES sub-systems to the hourly availability of thermal energy and the resulting grid electricity utilization required to supplement the on-site thermal energy generation. The relative sizing of the CST, PV, and TES sub-systems were determined by minimizing the LCOH. The sensitivity of the LCOH to various economic parameters was investigated and this paper shows the potential of the particle-TES for IPH applications. The methodology and tool described here can be readily extended and applied to particle TES systems for many potential IPH applications over various temperature conditions and can facilitate future techno-economic comparisons of particle-TES against alternative technologies for particular use cases (for example, parabolic trough or linear Fresnel systems for steam generation).

#### ACKNOWLEDGEMENTS

This work was authored by the National Renewable Energy Laboratory, operated by Alliance for Sustainable Energy, LLC, for the U.S. Department of Energy (DOE) under Contract No. DE-AC36-08GO28308. Funding provided by U.S. Department of Energy Office of Energy Efficiency and Renewable Energy Solar Energy Technologies Office and Office of Technology Transfer under Award Number 38394. The views expressed in the article do not necessarily represent the views of the DOE or the U.S. Government. The U.S. Government retains and the publisher, by accepting the article for publication, acknowledges that the U.S. Government retains a nonexclusive, paid-up, irrevocable, worldwide license to publish or reproduce the published form of this work, or allow others to do so, for U.S. Government purposes.

#### REFERENCES

- [1] U.S. Environmental Protection Agency, 2020, “Industry Sector Emissions.”
- [2] Locatelli, G., and Mancini, M., 2011, *Emergency Planning Zone: Constraints and Opportunities for the Development of Nuclear Energy and Exploitation of Its Process Heat*. doi: 10.13140/2.1.3657.5362.
- [3] Schoeneberger, C. A., McMillan, C. A., Kurup, P., Akar, S., Margolis, R., and Masanet, E., 2020, “Solar for Industrial Process Heat: A Review of Technologies, Analysis Approaches, and Potential Applications in the United States,” *Energy*, **206**, p. 118083.
- [4] McMillan, C. A., and Ruth, M., 2019, “Using Facility-Level Emissions Data to Estimate the Technical Potential of Alternative Thermal Sources to Meet Industrial Heat Demand,” *Appl. Energy*, **239**, pp. 1077–1090.
- [5] Ma, Z., Davenport, P., and Zhang, R., 2020, “Design Analysis of a Particle-Based Thermal Energy Storage System for Concentrating Solar Power or Grid Energy Storage,” *J. Energy Storage*, **29**, p. 101382.
- [6] Energy, U. S. D. of, “Technology Strategy Assessment - Thermal Energy Storage” [Online]. Available: <https://www.energy.gov/oe/storage-innovations-2030>. [Accessed: 09-Dec-2023].
- [7] Aguilar-Jiménez, J. A., Velázquez, N., Acuña, A., Cota, R., González, E., González, L., López, R., and Islas, S., 2018, “Techno-Economic Analysis of a Hybrid PV-CSP System with Thermal Energy Storage Applied to Isolated Microgrids,” *Sol. Energy*, **174**, pp. 55–65.
- [8] Immonen, J., and Powell, K. M., 2022, “Dynamic Optimization with Flexible Heat Integration of a Solar Parabolic Trough Collector Plant with Thermal Energy Storage Used for Industrial Process Heat,” *Energy Convers. Manag.*, **267**, p. 115921.
- [9] Stuber, M., 2018, “A Differentiable Model for Optimizing Hybridization of Industrial Process Heat Systems with Concentrating Solar Thermal Power,” *Processes*, **6**(7), p. 76.

- [10] Crespo, A., Barreneche, C., Ibarra, M., and Platzer, W., 2019, "Latent Thermal Energy Storage for Solar Process Heat Applications at Medium-High Temperatures – A Review," *Sol. Energy*, **192**, pp. 3–34.
- [11] Mohammadi, K., Khanmohammadi, S., Immonen, J., and Powell, K., 2021, "Techno-Economic Analysis and Environmental Benefits of Solar Industrial Process Heating Based on Parabolic Trough Collectors," *Sustain. Energy Technol. Assessments*, **47**, p. 101412.
- [12] Rashid, K., Mohammadi, K., and Powell, K., 2020, "Dynamic Simulation and Techno-Economic Analysis of a Concentrated Solar Power (CSP) Plant Hybridized with Both Thermal Energy Storage and Natural Gas," *J. Clean. Prod.*, **248**, p. 119193.
- [13] Temiz, M., and Dincer, I., 2021, "Concentrated Solar Driven Thermochemical Hydrogen Production Plant with Thermal Energy Storage and Geothermal Systems," *Energy*, **219**, p. 119554.
- [14] Beck, A., Sevault, A., Drexler-Schmid, G., Schöny, M., and Kauko, H., 2021, "Optimal Selection of Thermal Energy Storage Technology for Fossil-Free Steam Production in the Processing Industry," *Appl. Sci.*, **11**(3), p. 1063.
- [15] Mcmillan, C., Boardman, R., Mckellar, M., Sabharwall, P., Ruth, M., and Bragg-Sitton, S., 2016, *Generation and Use of Thermal Energy in the U.S. Industrial Sector and Opportunities to Reduce Its Carbon Emissions*.
- [16] Davenport, P., Martinek, J., and Ma, Z., 2019, "Analysis of Concentrating Solar Thermal System to Support Thermochemical Energy Storage or Solar Fuel Generation Processes," *ASME 2019 13th International Conference on Energy Sustainability*, American Society of Mechanical Engineers.
- [17] Ma, Z., Zhang, R., and Sawaged, F., 2017, "Design of Particle-Based Thermal Energy Storage for a Concentrating Solar Power System," *ASME 2017 11th International Conference on Energy Sustainability*, American Society of Mechanical Engineers.
- [18] Ge, Z., Li, Y., Li, D., Sun, Z., Jin, Y., Liu, C., Li, C., Leng, G., and Ding, Y., 2014, "Thermal Energy Storage: Challenges and the Role of Particle Technology," *Particuology*, **15**, pp. 2–8.
- [19] Mohan, G., Venkataraman, M. B., and Coventry, J., 2019, "Sensible Energy Storage Options for Concentrating Solar Power Plants Operating above 600 °C," *Renew. Sustain. Energy Rev.*, **107**(November 2017), pp. 319–337.
- [20] Prieto, C., and Cabeza, L. F., 2019, "Thermal Energy Storage (TES) with Phase Change Materials (PCM) in Solar Power Plants (CSP). Concept and Plant Performance," *Appl. Energy*, **254**(January), p. 113646.
- [21] González-Portillo, L. F., Albrecht, K., and Ho, C. K., 2021, "Techno-Economic Optimization of CSP Plants with Free-Falling Particle Receivers," *Entropy*, **23**(1), pp. 1–24.
- [22] Reyes-Belmonte, M. A., Díaz, E., Romero, M., and González-Aguilar, J., 2018, "Particles-Based Thermal Energy Storage Systems for Concentrated Solar Power," p. 210013.
- [23] González-Portillo, L. F., Albrecht, K. J., Sment, J., Mills, B., and Ho, C. K., 2022, "Sensitivity Analysis of the Levelized Cost of Electricity for a Particle-Based Concentrating Solar Power System," *J. Sol. Energy Eng. Trans. ASME*, **144**(3), pp. 1–8.
- [24] Trevisan, S., Guédez, R., and Laumert, B., 2020, "Thermo-Economic Optimization of an Air Driven Supercritical CO<sub>2</sub> Brayton Power Cycle for Concentrating Solar Power Plant with Packed Bed Thermal Energy Storage," *Sol. Energy*, **211**(November), pp. 1373–1391.
- [25] Buck, R., Agrafiotis, C., Tescari, S., Neumann, N., and Schmücker, M., 2021, "Techno-Economic Analysis of Candidate Oxide Materials for Thermochemical Storage in Concentrating Solar Power Systems," *Front. Energy Res.*, **9**(July), pp. 1–13.
- [26] Gorman, B. T., Lanzarini-Lopes, M., Johnson, N. G., Miller, J. E., and Stechel, E. B., 2021, "Techno-Economic Analysis of a Concentrating Solar Power Plant Using Redox-Active Metal Oxides as Heat Transfer Fluid and Storage Media," *Front. Energy Res.*, **9**, pp. 1–18.
- [27] Ma, Z., Gifford, J., Wang, X., and Martinek, J., 2023, "Electric-Thermal Energy Storage Using Solid Particles as Storage Media," *Joule*, **7**(5), pp. 843–848.
- [28] Al-Ghussain, L., Alrbai, M., Al-Dahidi, S., Lu, Z., and Lee, P., 2024, "Techno-Economic and Environmental Assessment of Solar-Based Electrical Vehicles Charging Stations Integrated with Hydrogen Production," *J. Clean. Prod.*, **434**, p. 140219.
- [29] Mills, B. H., Ho, C. K., Schroeder, N. R., Shaeffer, R., Laubscher, H. F., and Albrecht, K. J., 2022, "Design Evaluation of a Next-Generation High-Temperature Particle Receiver for Concentrating Solar Thermal Applications," *Energies*, **15**(5), p. 1657.
- [30] Solar Energy Technologies Office, U. D. of E. (DOE), 2021, "2030 Solar Cost Targets."
- [31] Al-Ghussain, L., Darwish Ahmad, A., Abubaker, A. M., and Hassan, M. A., 2022, "Techno-Economic Feasibility of Thermal Storage Systems for the Transition to 100% Renewable Grids," *Renew. Energy*, **189**, pp. 800–812.
- [32] Ma, Z., Wang, X., Davenport, P., Gifford, J., and Martinek, J., 2022, "Preliminary Component Design and Cost Estimation of a Novel Electric-Thermal Energy Storage System Using Solid Particles," *J. Sol. Energy Eng.*, **144**(3).
- [33] Ma, Z., Wang, X., Davenport, P., Gifford, J., Cook, K., Martinek, J., Schirck, J., Morris, A., Lambert, M., Zhang, R, 2022, "System and component development for long-duration energy storage using particle thermal energy storage" *Applied Thermal Engineering* 21, p. 119078.
- [34] National Renewable Energy Laboratory (NREL), "National Solar Radiation Database."
- [35] California ISO Open Access Same-time Information System (OASIS), "Locational Marginal Prices (LMP)."